

A NOTE ON THE APPLICATION OF LINEAR WAVE THEORY AT A CRITICAL LEVEL

ANDREAS DÖRNBRACK

*DLR, Institut für Physik der Atmosphäre,
D – 82230 Oberpfaffenhofen, Germany*

CARMEN J. NAPPO

*Atmospheric Turbulence and Diffusion Division Air Resources Laboratory/NOAA
456 S. Illinois Ave, Oak Ridge, TN 37831, USA*

(Received in final form 23 August, 1996)

Abstract. The purpose of this note is to estimate the accuracy and practical limitations of applying linear theory at a critical level over a realistic range of atmospheric stabilities for an idealized surface terrain. These estimates are made by comparing the results of a linear model with a nonlinear numerical model at a critical level. Essentially similar results are obtained from each model for wave stress, wave breaking height and wave dissipation through the critical level. Because gravity waves can be either evanescent or internal depending on the relative sizes of the Scorer parameter and the wavenumber of the ground surface disturbance, the somewhat paradoxical result develops that wave breaking and non-linearity increase with increasing bulk Richardson number. It is recommended that steady linear wave theory be used in gravity wave drag parameterizations provided near real time profiles of background velocity and temperature are available.

Key words: Stratified flows, Critical Level, Linear Wave Theory, Numerical Simulations

1. Introduction

The importance of the effects of gravity waves on almost all scales of geophysical flows is widely recognized. One of the most important of these effects is the vertical transport and deposition of wave-generated stress. Wave stress can be created when a statically stable fluid flows over a surface terrain obstacle. Inviscid linear theory predicts the stress to propagate upward with a constant value (Eliassen and Palm, 1960). For sheared flow, the wave stress will be attenuated at a critical level where the wave horizontal phase speed equals the background flow velocity. The linear theory cannot describe the attenuation process, but it is assumed that the wave stress is transferred to the background flow through the generation of turbulence in a layer immediately below the critical level. This wave-generated turbulence is not accounted for in conventional turbulence theory; however, much work has been directed toward the parameterization of this turbulence in numerical models (see, for example, Kim and Arakawa, 1995; Fritts, 1984).

These parameterizations are almost always based on the linear theory. However, linear theory is really only applicable when the wave amplitudes are sufficiently small such that the products of wave quantities are negligible. Obviously, if the wave amplitude grows so as to create an instability of the background flow, as is the

case when a wave approaches a critical level, then it is not clear that the assumption of linearity still holds. In such a case, when nonlinear terms become large, how accurate are the wave quantities calculated with the linear theory?

The purpose of this note is to estimate the accuracy and practical limitations of applying the linear theory at a critical level over a realistic range of atmospheric conditions and surface terrains. These estimates will be made by comparing the results of a linear theory model with a nonlinear numerical model at a critical level. In Section 2, we highlight the behaviour of a gravity wave at a critical level. In Section 3, we briefly describe the linear and the numerical models. In Section 4 we describe the procedures of the calculations, and in Section 5 we present the results of these comparisons. A discussion on the implications of these results is given in Section 6, and in Section 7 we present our conclusions and recommendations.

2. Wave behaviour at a critical level

The result of linearizing the Eulerian equations governing atmospheric flow, making the Boussinesq approximation, and assuming a horizontal wave structure for the perturbations of the background flow is the Taylor-Goldstein equation:

$$\hat{w}_{zz} + \left[\frac{N^2}{(U - c)^2} - k^2 \right] \cdot \hat{w} = 0, \quad (1)$$

where \hat{w} is the Fourier transform of the wave-induced vertical velocity, $N(z)$ is the buoyancy frequency, $U(z)$ is the background wind, c is the horizontal phase velocity, and k is the horizontal wavenumber of the wave, and the subscript indicates differentiation. When $U(z_c) = c$, Equation (1) becomes singular, and the height z_c is called a critical level. The behaviour of a gravity wave at a critical level has been studied extensively by theoretical means; however, relatively few laboratory studies have been performed (Thorpe, 1981; Koop and McGee, 1986; Delisi and Dunkerton, 1989), and even fewer direct observations in the atmosphere and oceans (Merrill and Grant, 1979; Worthington and Thomas, 1996). Booker and Bretherton (1967) used linear inviscid theory to demonstrate that as a gravity wave propagates through the critical level, its amplitude is reduced by a factor $\exp \left\{ -2\pi(Ri_c - 0.25)^{1/2} \right\}$, where $Ri_c (> 0.25)$ is the Richardson number at the critical level. Hazel (1967) extended this analysis to include the effects of viscosity and heat conductivity, thus removing the singularity at the critical level. He recovered the same attenuation factor as for the inviscid case, but more significant is the result that “viscosity is important only in a critical layer around the critical level, a layer thicker below the critical level than above it (for upward propagating waves)”. The viscous length scale is defined by $z_\nu = (\nu/kU_z)^{1/3}$ where ν is the fluid viscosity, and U_z is the background wind shear at the critical level. The total thickness of the critical layer is estimated to be about $7z_\nu$, with $5z_\nu$ lying below the critical

level. Hazel (1967) shows that for the atmosphere and a wave of horizontal length of 10 km, z_ν is about 1 m. The inviscid theory predicts a discontinuous reduction of wave amplitude across the critical level, but the viscous theory predicts a linear decrease in wave amplitude through a layer of thickness several z_ν .

Thorpe (1981) compares laboratory experiments with an inviscid, non-diffusive, weakly nonlinear wave model. The waves are produced in the accelerating flow of a stratified fluid in a long tilted tube in which the lower boundary has a sinusoidal corrugation. The numerical model is used to provide information on the velocity distribution that cannot be measured easily or accurately in the experiments. Model verification or accuracy is assumed when there is agreement between the model results and the measured quantities such as wave amplitude and phase. Experimental results indicate that fluid viscosity acts to inhibit Kelvin-Helmholtz instability near the critical level. They observe that for mean flow $Ri \approx 1.5$, the waves become distorted from the linear theory solution profile. The second-order terms account for much of the distortion until $Ri \approx 0.5$ in the accelerating flow or until overturning becomes imminent. They use the numerical solution to calculate local Ri , and use these values to define regions of either dynamic or convective instability.

It is clear that the physics of the wave-turbulence exchange process at a critical level are complicated, and beyond the scope of linear theory. In a parameterization of the transfer of stress between a wave and the mean flow, it is necessary to calculate not only the wave stress but also the distance over which the stress is dissipated, i.e. the thickness of the layer of largest stress divergence. Inviscid linear theory, which we wish to use, can be used to calculate the distance, $z_c - z_{break}$ from the critical level where wave breaking first occurs. For example, we define z_{break} as the height where the total horizontal velocity is zero; note this is also the height where the flow streamlines become vertical. We can then assume that the wave stress decreases linearly from there to the critical level, and that the stress at the critical level is some fraction of its initial value. However, this assumption must be tested, and this is done in our study.

3. Numerical and linear models

In this section we give brief descriptions of the numerical and linear models used in the study. Because we evaluate the linear model relative to the nonlinear numerical model, we show first some comparisons of the numerical model with laboratory results. These comparisons serve to validate the numerical model.

3.1. LINEAR WAVE MODEL

The linear model solves Equation (1) with $c = 0$ since the surface-generated gravity wave is stationary relative to the ground surface. The bottom boundary condition is $\hat{w} = kU(0) \sin(kx)$, and at the top of the model we impose the

radiation condition, i.e. only upward propagating wave energy. The horizontally-averaged wind and temperature profiles calculated by the numerical model are used as the input background profiles for the wave model at a given time. Details of the calculations and treatment of the critical level are described in Nappo and Chimonas (1992); however, in the present case integration over a range of horizontal wavenumbers is unnecessary because the wave forcing is at a single wavenumber $k = 2\pi/\lambda$.

3.2. NUMERICAL MODEL AND COMPARISON WITH A LABORATORY EXPERIMENT

The numerical simulations consider a two-dimensional (x, z) shear flow in a thermally stratified fluid with constant buoyancy frequency $N^2 = g/\vartheta_0 d\Theta/dz$, where $\Theta(z)$ is the mean part of the total temperature profile $\vartheta = \vartheta_0 + \Theta + \theta$, and ϑ_0 is a reference temperature at the ground surface. The numerical scheme integrates the full primitive equations of motion in their non-hydrostatic form as a function of time. The Boussinesq approximation is employed. Additionally, we solve an equation for the temperature fluctuations as an appropriate form of the first law of thermodynamics. A gravity wave is excited by flow over a sinusoidal ground surface with wavelength λ and amplitude δ . The domain size in the horizontal direction is λ and the height is H . Details of the equations and the numerical scheme are given in Dörnbrack et al. (1995). A further application to the three-dimensional gravity-wave critical-level interaction is presented in Dörnbrack (1996).

Dörnbrack et al. (1995) presented a comparison of preliminary model results with observations of the laboratory experiment of Thorpe (1981). There, the initial velocity distribution and the mean temperature field were prescribed by

$$U(z) = \bar{S}(z - 0.5H), \quad \frac{\Theta(z)}{\vartheta_0} = \frac{\Delta\Theta}{\vartheta_0} \frac{(z - 0.5H)}{H}, \quad (2)$$

where the dimensionless temperature gradient was $\Delta\Theta/\vartheta_0 = N^2H/g$ and the mean shear \bar{S} was calculated by means of $\bar{S} = N^2t_\alpha \sin \alpha_0$ (Thorpe, 1968). The values of the buoyancy frequency N , the tilting angle α_0 , and the time of tilting t_α were taken from the data of Figure 4 of Thorpe (1981). Thus, Dörnbrack et al. (1995) did not consider the actual tilting process. They initialised the numerical model with the already fully developed flow profile and consequently they must correct the time scale of the simulation by the value of t_α in order to compare their results with the findings of Thorpe (1981).

Here, we present new results of the same case in which the correct process of tilting is taken into account. The tube is tilted down to an angle $\alpha_0 = 7.06^\circ$ for a period of 0.503 s, is kept at this position for 3.480 s, and is returned to the horizontal position in 0.345 s (personal communication by Thorpe, 1994).

For simulating the tilting, the buoyancy term $\theta/\vartheta_0\delta_{3i}$ in the momentum balance (Equation 4 in Dörnbrack et al., 1995) takes now the form

$$\left(\frac{\Theta + \theta}{\vartheta_0} \sin(\alpha(t)), 0, \frac{\Theta + \theta}{\vartheta_0} \cos(\alpha(t)) \right), \quad (3)$$

where we approximate the tube tilting by a time dependent angle $\alpha(t)$ according to

$$\frac{\alpha(t)}{\alpha_0} = \begin{cases} 0.5 \left(1 - \cos(\pi \frac{t}{t_1}) \right) & \implies 0 \leq t \leq t_1 = 0.503 \text{ s} \\ 1 & \implies t_1 < t < t_2 = 3.983 \text{ s} \\ 0.5 \left(1 + \cos(\pi \frac{t-t_2}{t_3-t_2}) \right) & \implies t_2 \leq t \leq t_3 = 4.328 \text{ s} . \end{cases} \quad (4)$$

As in Dörnbrack et al. (1995), the initial velocity and temperature fluctuations are set to zero and the same numerical resolution (200x128 grid cells) and the same boundary conditions are used.

We compare our results with observations of Thorpe (1981) in Figure 1. In the observations, layers of constant density were marked by adding dye. Initially, these layers have an equal thickness depending on the experimental set-up in the laboratory. For a quantitative comparison with measurements, we plot the contour lines of the temperature field in such a way that the thickness and position of the areas between adjacent contour lines correspond to the black and white layers documented in the photograph of the observations at $t = 0$ (Figure 1a). At the beginning, the lines of constant temperature are horizontal, i.e., colder fluid is lying in the trough and the fluid becomes warmer with increasing height. The mean flow is towards the left near the bottom boundary and towards the right at the top boundary. The overall features of the flow evolution in the laboratory and in the numerical simulation are similar. The sinusoidal corrugations at the bottom surface excite gravity waves that propagate vertically upwards (Figure 1b). The amplitudes of the waves increase with height, but fall to zero directly beneath the critical level. No wavy motion is found above this level. Regions of reduced vertical temperature gradients (characterized by thickening of the marked layers) are mainly found above the trough of the surface wave (Figures 1c and d). Because of the reduced temperature gradients, the local Richardson number drops, and these regions become convectively unstable. These are the locations where wave-induced advection puts colder fluid over warmer ones (Figure 1e) leading to the wave overturning. Between these sites of instability the vertical temperature gradient is enhanced and the black and white areas above the crest of the surface become thinner, a structure similar to that found for Kelvin-Helmholtz instability.

A slight difference is seen between the observed and computed results for the horizontal position of the white unstable region over the trough. As mentioned before, this position is influenced by the momentum transfer between wave and mean flow. The resulting acceleration of the mean flow depends on viscosity. The lower the Reynolds number, the weaker the momentum transferred from the wave to the mean flow in agreement with findings of Fritts and Geller (1976). Thus,

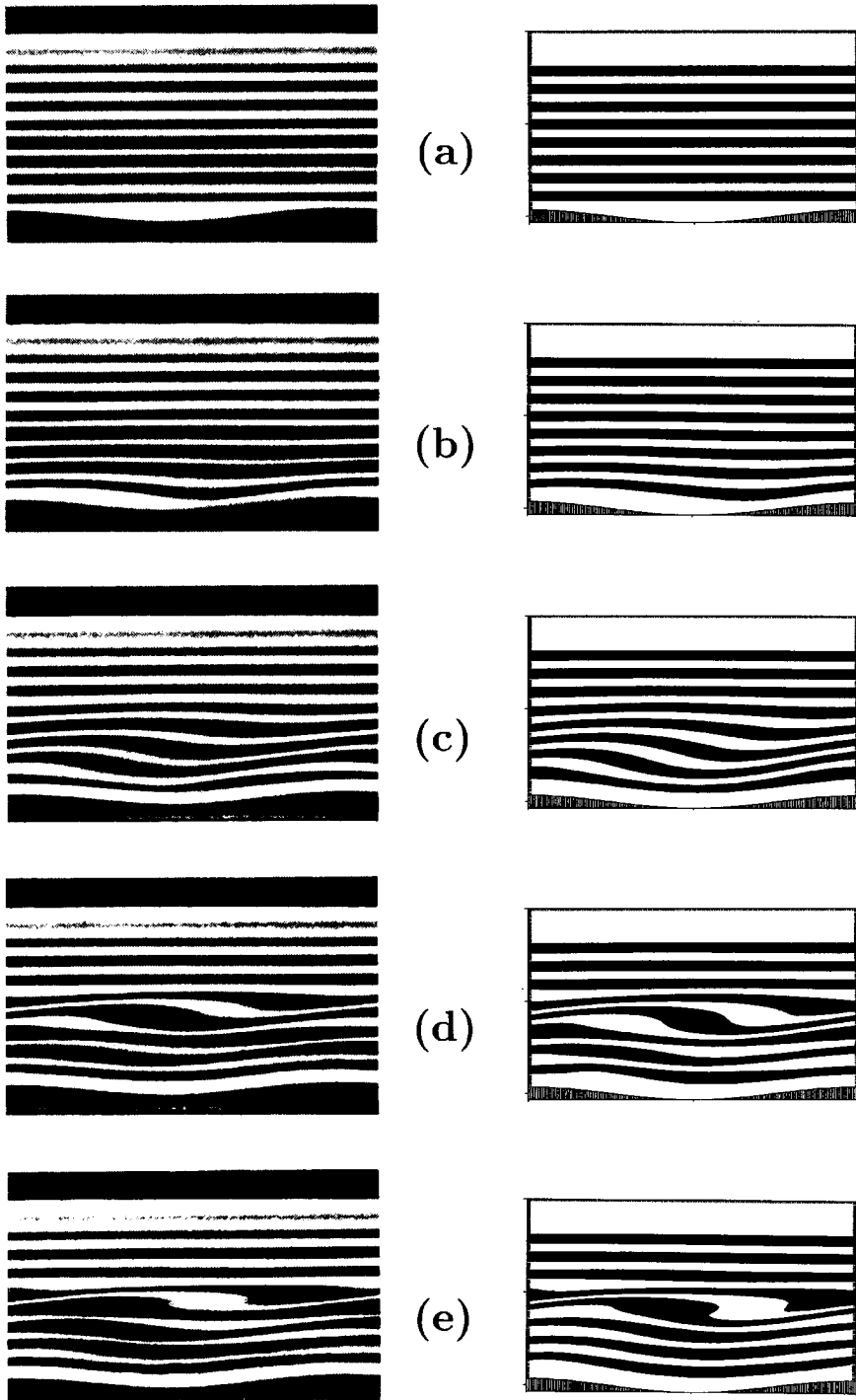


Figure 1. Comparison with the observations of Thorpe (1981, Figure 4a,c,e,h,j). Left side: experimental results at $t = 0$ s (a), $t = 2.2$ s (b), and $t = 4.5$ s (c), $t = 7.9$ s (d), and $t = 10.2$ s (e). Right side: Results of the numerical simulation at corresponding times.

a too large Reynolds number might be the reason for this deviation. Although we have not used the same boundary conditions in the experiment (no friction), excellent agreement with the observed flow patterns was obtained. Obviously, the viscous friction at the top and bottom surface is of minor importance in this case as discussed in Dörnbrack et al. (1995).

Baines (1995) describes two actions that can occur when a gravity wave encounters a critical level when U and N vary gradually with height and the Richardson number is larger than one quarter. If the wave approaches the critical level slowly, the viscous dissipation in the critical layer may be large enough to prevent explosive wave growth and overturning. In this case, the wave never reaches the critical level. However, if the wave approaches the critical level quickly, substantial wave overturning occurs resulting in a homogeneous mixed layer. Our results suggest that the latter action is taking place in the tank experiment of Thorpe and in the non-linear model simulations.

4. Procedure

The numerical simulations we are going to discuss in the next section start with the profiles given by Equation (2). The buoyancy frequency is $N = 2 \text{ s}^{-1}$ in all runs, and the surface wavelength $\lambda = 2H$. Because we vary the mean shear \bar{S} , the actual flow regime can be described in terms of a bulk Richardson number

$$Ri_B = \frac{N^2}{\bar{S}^2} = \frac{N^2 H^2}{\Delta U^2} = \frac{g\Delta\Theta H}{\vartheta_0 \Delta U^2}, \quad (5)$$

and the dimensionless amplitude δ/H of the surface wave. Table I gives an overview of the parameters used in our simulations, and all eight cases are run for four values of $\delta/H = 0.005, 0.010, 0.015, 0.020$. Because of the z -dependent velocity profile, the Scorer parameter $\ell = N/|U|$ increases with height. The ratio

$$\gamma = \frac{k}{\ell}, \quad \text{where} \quad k = \frac{2\pi}{\lambda} \quad (6)$$

determines the character of linear gravity waves. If $\gamma > 1$, i.e. if the intrinsic frequency Uk is large compared to the buoyancy frequency N , the buoyancy has little effect on the flow and the streamlines are in phase with the underlying topography. These waves are called evanescent since their amplitude is decreasing exponentially with height. For increasing stability, or similarly for decreasing flow speed, the ratio γ becomes less than one, i.e. the intrinsic frequency Uk becomes less than N , and the waves are able to propagate vertically. These waves are called internal gravity waves. The surface value, γ_S , of this ratio is important because it characterizes the waves excited at ground. Because $|U(z=0)| = \Delta U/2$, the surface value γ_S can be easily derived from Equation (6) using Equation (5) as

$$\gamma_S = \frac{2\pi \Delta U/2}{\lambda N} = \sqrt{\frac{Ri_{IGW}}{Ri_B}}, \quad (7)$$

Table I
Simulation parameters

Run	ΔU (m s ⁻¹)	Ri_B	γ_S	z_{IGW}/H
1	0.05	40.96	0.24	-1.54
2	0.10	10.24	0.49	-0.52
3	0.15	4.55	0.74	-0.18
4	0.20	2.56	0.98	0
5	0.25	1.64	1.23	0.09
6	0.30	1.13	1.47	0.16
7	0.35	0.84	1.72	0.21
8	0.40	0.64	1.96	0.24

where $Ri_{IGW} \equiv \pi^2/(\lambda/H)^2 \approx 2.467$ determines the lower limit for Ri_B above which internal gravity waves are directly excited at the surface. Values of γ_S are listed in the third column of Table I. For $Ri_B < Ri_{IGW}$, or in other words if $\gamma_S > 1$, evanescent waves are excited at the bottom surface and the transition to internal gravity waves occurs in the bulk of the fluid at heights

$$z_{IGW} \geq 0.5H \left(1 - \gamma_S^{-1}\right). \quad (8)$$

This number is listed in the fourth column in Table I. All simulations are run until $t = 25 t_{ref}$, where $t_{ref} = H/\Delta U$.

5. Results

5.1. FLOW STRUCTURE

In this section, we describe the flow structures calculated by the numerical model. This analysis is necessary for a better understanding of the flow physics and the differences between the linear and numerical model results. Contour lines of ϑ/ϑ_0 are plotted in Figure 2 for different values of Ri_B at $t = 25 t_{ref}$, and $\delta/H = 0.015$. Runs for smaller values of δ/H did not show wave breaking. In all cases, wave activity is seen below the critical level, and horizontal, almost undisturbed flow above $z \approx 0.5H$. The temporal evolution of the flow shown in Figure 2 is similar to that described in Section 3.2. Below the critical level, the dependence of flow stability on Ri_B is clearly illustrated; the tendency for wave breaking increases with increasing Ri_B . Also seen in Figure 2 is a sinking of the breaking level, z_{break} , with increasing Ri_B . Normally, we expect increasing flow stability with increasing bulk Richardson number. However, when gravity waves are present and a critical level exists, the flow stability becomes a complicated function of wave perturbation amplitudes and mean flow quantities. As we have seen in the previous section, when $Ri_B > Ri_{IGW}$, an internal gravity wave with the same amplitude as

the surface wave is excited, but when $Ri_B < Ri_{IGW}$, an evanescent gravity wave with amplitude decreasing exponentially with height is excited. Near the critical level, $U(z)$ becomes small, and the Scorer parameter, ℓ , becomes large. Eventually, ℓ becomes greater than k , and the wave switches to internal at $z = z_{IGW}$, but now the wave amplitude is much reduced from its original value. Because the wave stress is quadratic in wave amplitude, the reduced wave interacts weakly with the mean flow. The result is that the momentum transfer at the critical layer is a function of the bulk Richardson number.

An indication of the different amounts of momentum that are transferred to the mean flow is the position of the unstable region relative to the surface wave. In Figure 2, it is seen that the region of instability is shifted towards the positive x -direction with increasing Ri_B indicating an increasing wave-induced acceleration of the mean flow below the critical level.

The dimensionless height of wave breaking z_{break}/H at time $15 t_{ref}$ is plotted as a function of bulk Richardson number, Ri_B , in Figure 3. For the linear model, z_{break} is determined as the height where the total velocity first becomes zero, and for the numerical model z_{break} is determined as that height where the flow streamlines first become vertically orientated. These definitions are equivalent if we take the total horizontal velocity as $U + u' = d\zeta/dz$ where ζ is the flow streamline. The numerical and linear models both predict an approximately exponential decrease of z_{break} with increasing Ri_B . The linear model uses the vertical profiles of mean velocity and temperature calculated by the numerical model at $15 t_{ref}$. It is also seen that as Ri_B approaches zero, z_{break} approaches $0.5H$, and that z_{break} decreases with increasing δ/H for all Ri_B .

The flow structures at $t = 25 t_{ref}$ for different values of δ/H and for low and high Ri_B are shown in Figure 4. As expected, the stronger excitation of gravity waves due to higher surface wave amplitudes results in regions of increasing instability, i.e., the separation between the contour lines becomes wider up to the point when the flow becomes convectively unstable; clearly visible is the different behaviour of the wave overturning for $Ri_B = 0.84$ and 10.24 .

5.2. MOMENTUM FLUX NEAR THE GROUND SURFACE

In Figure 5, the dimensionless momentum flux, $\tau_S/\rho_0\Delta U^2$, close to the bottom surface is plotted for early and late times as a function of Ri_B . Contributions to this flux at height z are the resolved motions and the modelled fluxes of the frictional stresses. The latter are set to zero in order to compare our results with the inviscid linear theory. At undulated surfaces, however, pressure forces cause an additional momentum flux. Therefore, we compute the mean vertical momentum flux per unit volume τ at constant coordinate η where η is the height in terrain-following coordinates (see Dörnbrack and Schumann, 1993). Additionally, we take a mean over the lowest 20% of the total domain height because the vertical profiles of

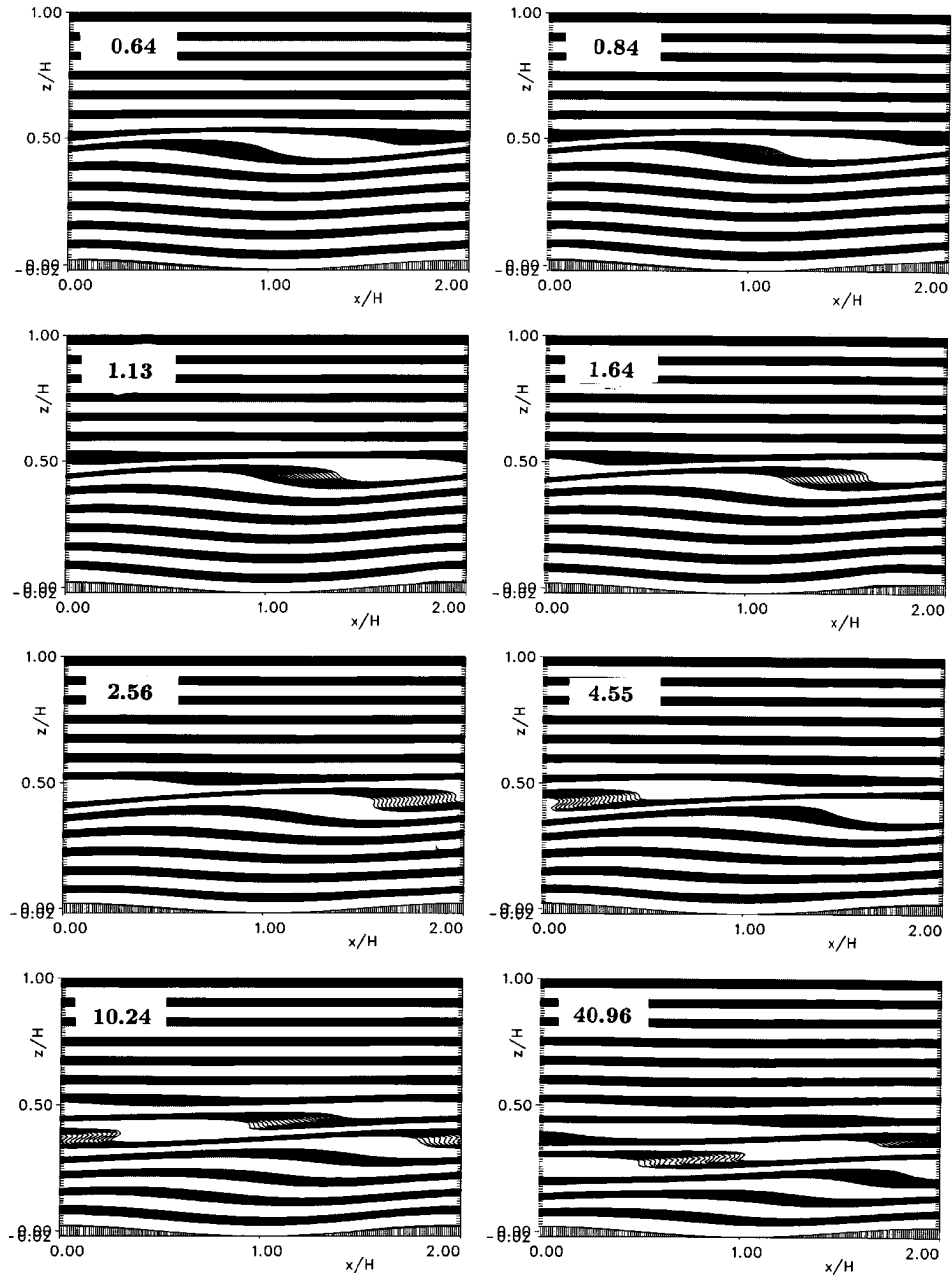


Figure 2. Flow structure at $t = 25t_{ref}$. Fixed $\delta/H = 0.015$. Parameter is the bulk Richardson number Ri_B .

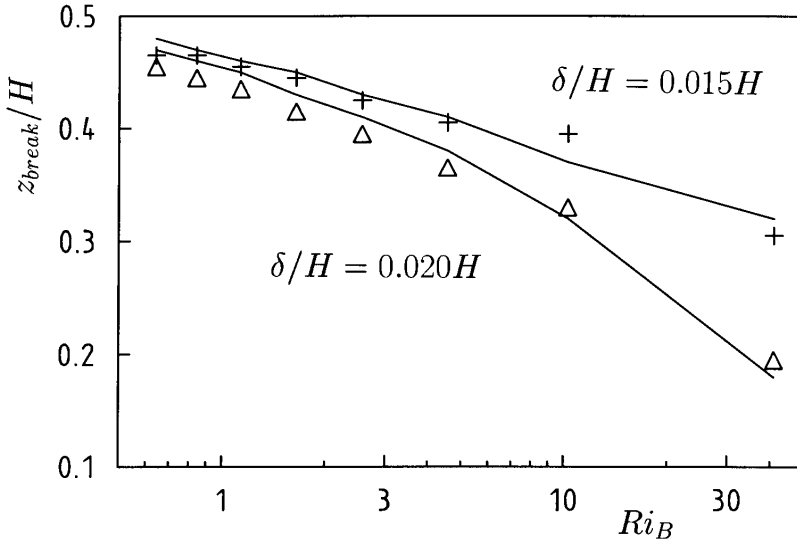


Figure 3. Breaking height at $t = 15t_{ref}$ as a function of Ri_B for $\delta/H = 0.015$ and $\delta/H = 0.020$. Symbols are results of the linear wave model. The lines are from the numerical model.

stress show a wavelike structure (see discussion of Figure 6 in Dörnbrack et al., 1995).

The linear wave theory for uniform constant flow of magnitude $\Delta U/2$ over a wavy surface predicts (see, for example, Smith, 1979)

$$\frac{\tau_S}{\rho_0 \Delta U^2} = \pi \frac{\delta}{\lambda} \frac{\delta}{H} \sqrt{Ri_B - Ri_{IGW}} \quad \text{for } Ri_B > Ri_{IGW}. \quad (9)$$

It must be noted, that for this shear-free situation the Richardson number Ri_B in Equation (9) can be interpreted only as a value for the ratio γ of Equation (7). Equation (9) is only written in such a form for comparison purposes as τ_S depends on Ri_B for the sheared case. It can be easily shown, that the vertical wavenumber

$$m = \sqrt{\ell^2 - k^2} = \frac{2}{H} \sqrt{(Ri_B - Ri_{IGW})} \quad (10)$$

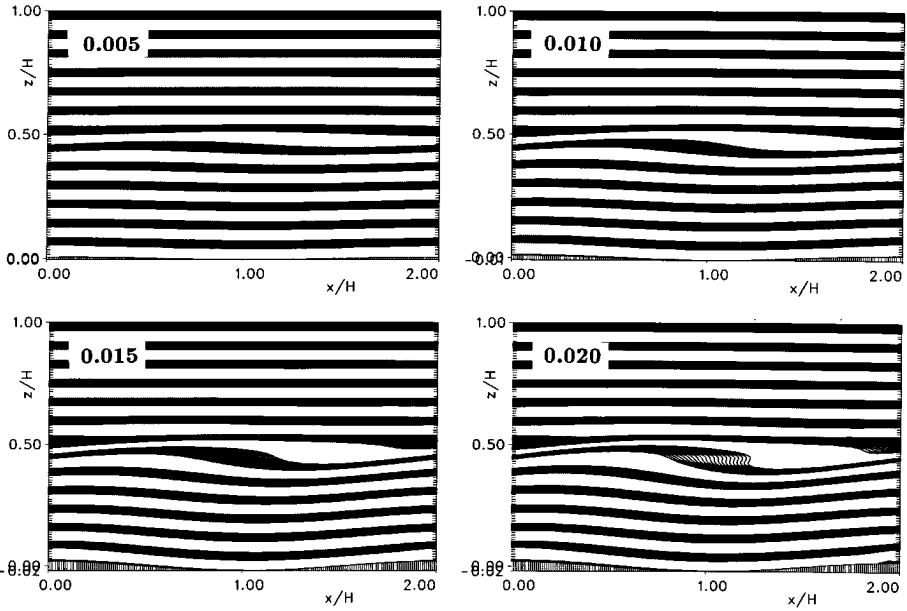
is imaginary for $Ri_B < Ri_{IGW}$, and the wave stress is zero. In the opposite case, when $Ri_B > Ri_{IGW}$ the stress is quadratic in terrain height, and for $Ri_B \approx Ri_{IGW}$ is $\tau_S \approx 0$.

Figure 5 shows the dependence of τ_S on Ri_B for early and late times in the simulation. For the early time, Figure 5a, the stress is a positive exponential function of Ri_B , for Ri_B less than about 10, with exponent $n \approx 2/3$. This suggests that

$$\frac{\tau_S}{\rho_0 \Delta U^2} \propto \delta^2 Ri_B^{2/3}. \quad (11)$$

The linear wave model gives essentially the same results as the numerical model. Unlike the case of uniform winds, the presence of a critical level ensures that there

(a)



(b)

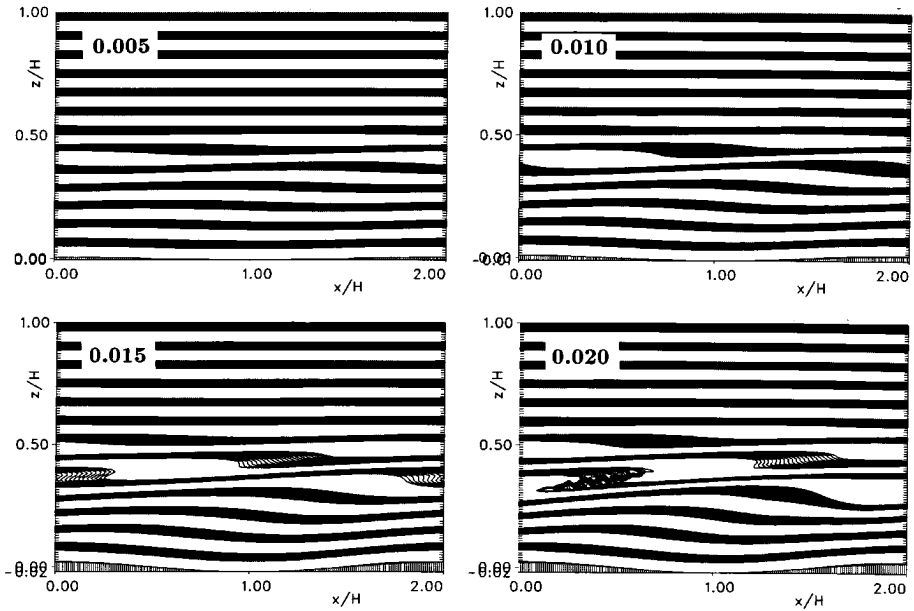


Figure 4. Flow structure at $t = 25 t_{ref}$ for $Ri_B = 0.84$ (a) and $Ri_B = 10.24$ (b). Parameter is the amplitude of the surface wave δ/H .

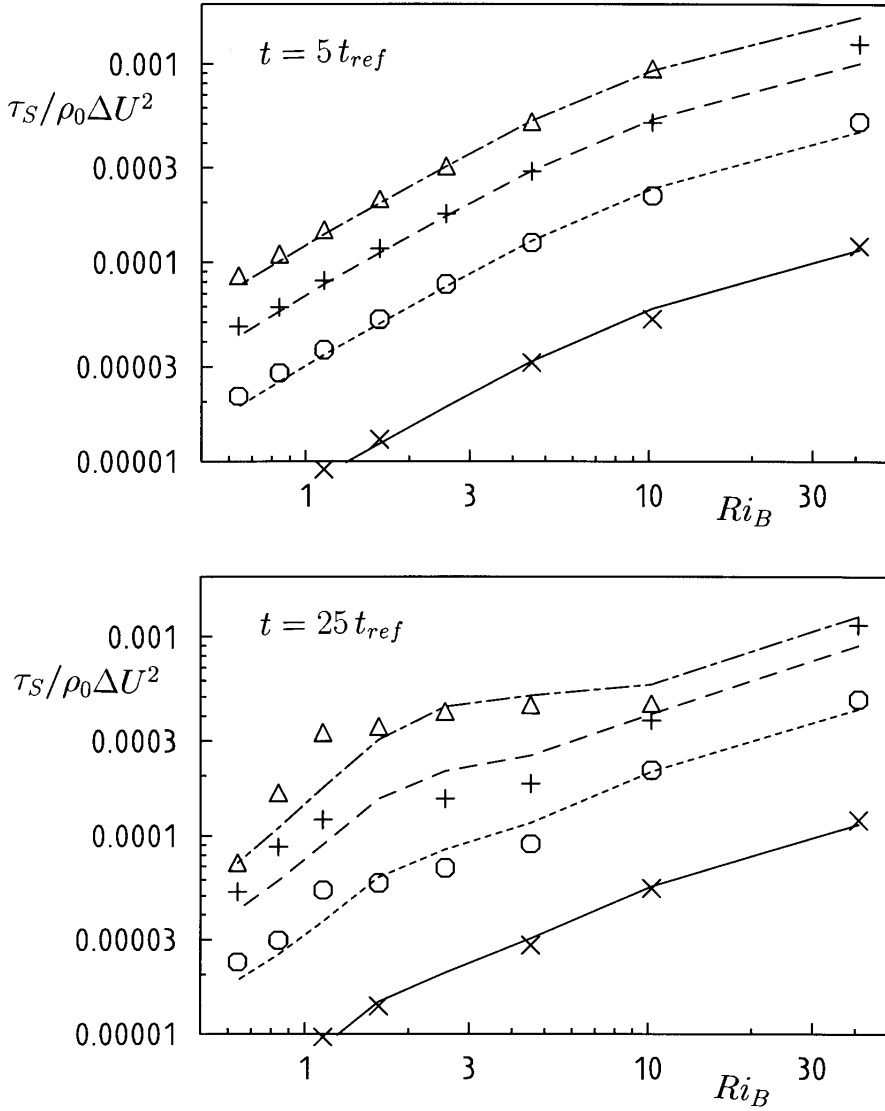


Figure 5. Surface momentum flux for different values of δ/H as a function of Ri_B at an early time $t = 5.0 t_{ref}$ (top) and at $t = 25 t_{ref}$ (bottom). Symbols are results of the linear wave model. The lines are from the numerical model and their codings are: $\delta/H = 0.005$ (—), 0.010 (---), 0.015 (-.-.-), 0.020 (.....).

will always be some wave stress, i.e. there will always be some region below the critical level where the gravity waves are internal. For later times, as shown in Figure 5b, the simple relation Equation (11) is applicable to only small terrain heights; however, it is seen that the linear model continues to follow the numerical

Table II
Wave reduction at the critical level

γ_S	Ri_c	Theory	Linear	Numerical
0.24	41	$3.9 \cdot 10^{-18}$	$3.9 \cdot 10^{-18}$	$2.0 \cdot 10^{-5}$
0.49	10	$2.4 \cdot 10^{-9}$	$2.4 \cdot 10^{-9}$	$2.0 \cdot 10^{-5}$
0.98	2.5	$7.2 \cdot 10^{-5}$	$3.5 \cdot 10^{-5}$	$3.5 \cdot 10^{-6}$
1.49	1.1	$2.7 \cdot 10^{-3}$	0	$4.5 \cdot 10^{-4}$
1.96	0.6	$2.0 \cdot 10^{-2}$	0	$4.3 \cdot 10^{-3}$

model. It has already been shown that wave breaking increase with increasing Ri_B , and this causes the complex behaviour seen in Figure 5b.

5.3. WAVE ATTENUATION ACROSS THE CRITICAL LEVEL

An important result of the linear theory is that as a gravity wave propagates through a critical level its amplitude is attenuated by an amount

$$\frac{\tau_+}{\tau_S} = \exp \left\{ -2\pi \sqrt{Ri_c - 0.25} \right\} \quad (12)$$

where τ_+ is the wave stress above the critical level, and Ri_c is the Richardson number at the critical level. If Ri_c is unity or larger, the attenuation is substantial, for example $4 \cdot 10^{-3}$ for $Ri_c = 1$ and $5 \cdot 10^{-6}$ for $Ri_c = 4$. A comparison of Equation (12) with the results of the linear and numerical model is presented in Table II. In Table II, Ri_B is used in Equation (12) instead of Ri_c . Because we use the mean profiles from the numerical model for the background conditions of the linear model, Ri_c can be different from Ri_B . In the numerical model, τ_+ is calculated as the mean between $\eta = 0.5H$ and $0.6H$. For large values of Ri_B , the linear model agrees with Equation (12), but the numerical model does not. From the discussion of Equation (7), it is seen that for this problem the gravity wave is evanescent near the bottom boundary when Ri_B is less than about 2.5. Thus, for low values Ri_B the internal wave amplitudes are small below the critical level, and are essentially zero above the critical level. The numerical model shows a different behaviour, i.e., relatively constant attenuation for large Ri_B , and greater attenuation than the linear model for small values of Ri_B .

When wave breaking occurs in the numerical model, the surface on which the total horizontal velocity is zero becomes convoluted and folds back on itself. Then the locations of the critical level and the values of Ri_c are not well defined. However, using the calculated values of wave attenuation an equivalent value, Ri_{ce} , of Ri_c can be estimated from Equation (12). Figure 6 shows the plots of Ri_{ce} as functions of Ri_B for dimensionless times of 5, 10, and 25. For early times (Figure 6a), Ri_{ce} is essentially independent of the amplitude of the surface wave, and weakly dependent on Ri_B . Consideration of Equation (11) and Figure 5 shows that

this behaviour is expected for early times before the onset of wave breaking. As time increases (Figure 6b), nonlinear effects begin to be seen, as indicated by an increased sensitivity of Ri_{ce} to δ/H . Finally, at the end of the simulation (Figure 6c), the non-linearity dominates, and the linear estimates of stress attenuation no longer apply.

6. Discussion

The purpose of this study was to evaluate the utility of linear wave theory in estimating gravity-wave generated stress and wave dissipation near a critical level. We have compared the results of a linear gravity-wave model with those obtained from a numerical simulation of laboratory flow experiments. We have provided evidence that the numerical model accurately reproduces the qualitative features of the Thorpe (1981) laboratory experiments, and more details of these simulations are given in Dörnbrack et al. (1995). Because of the limited measurement capability of the laboratory experiments, a quantitative analysis of wave stress and stress divergence is not possible. However, we feel that the numerical results are valid, and accurately reproduce the details of the laboratory flows. Whether the laboratory experiments or the simulations apply to the atmosphere remains uncertain.

Accepting this, we have demonstrated that the linear model gives essentially the same results as the nonlinear model when the time-dependent profiles of mean horizontal velocity and temperature calculated in the numerical code are used for the background conditions in the linear model. This is an important result because the linear model is applicable only to a flow that is slowly changing in time. Apparently, the gravity-wave structure in the numerical model (and by implication in the laboratory tank) sets up quickly enough so that from the perspective of the wave field the flow is nearly stationary. This observation has immediate impact on the parameterization of gravity-wave drag in atmospheric flow models especially at the meso- and microscale. For example, it can be argued that wave breaking and flow deceleration several hundred metres above the ground surface may be so rapid as to render linear theory inapplicable. This will most likely be the case when the background profiles used in the linear model are obtained by observation, say, an hour or more old. However, in a numerical model these background profiles are available every time step, and these can be used in a stationary linear wave model. Indeed, this approach has been used by Nappo and Andrén (1995) in their parameterization of boundary-layer wave drag. The results presented here suggest that wave drag parameterizations using linear theory and model-calculated background profiles are valid.

Another interesting result of this study is given by Equation (11) and shown in Figure 5a. In the atmosphere, the magnitude of the large-scale bulk Richardson number is often in the range between 1 and 10, and so the exponential relation given in Equation (11) might be a practical means of estimating the wave stress

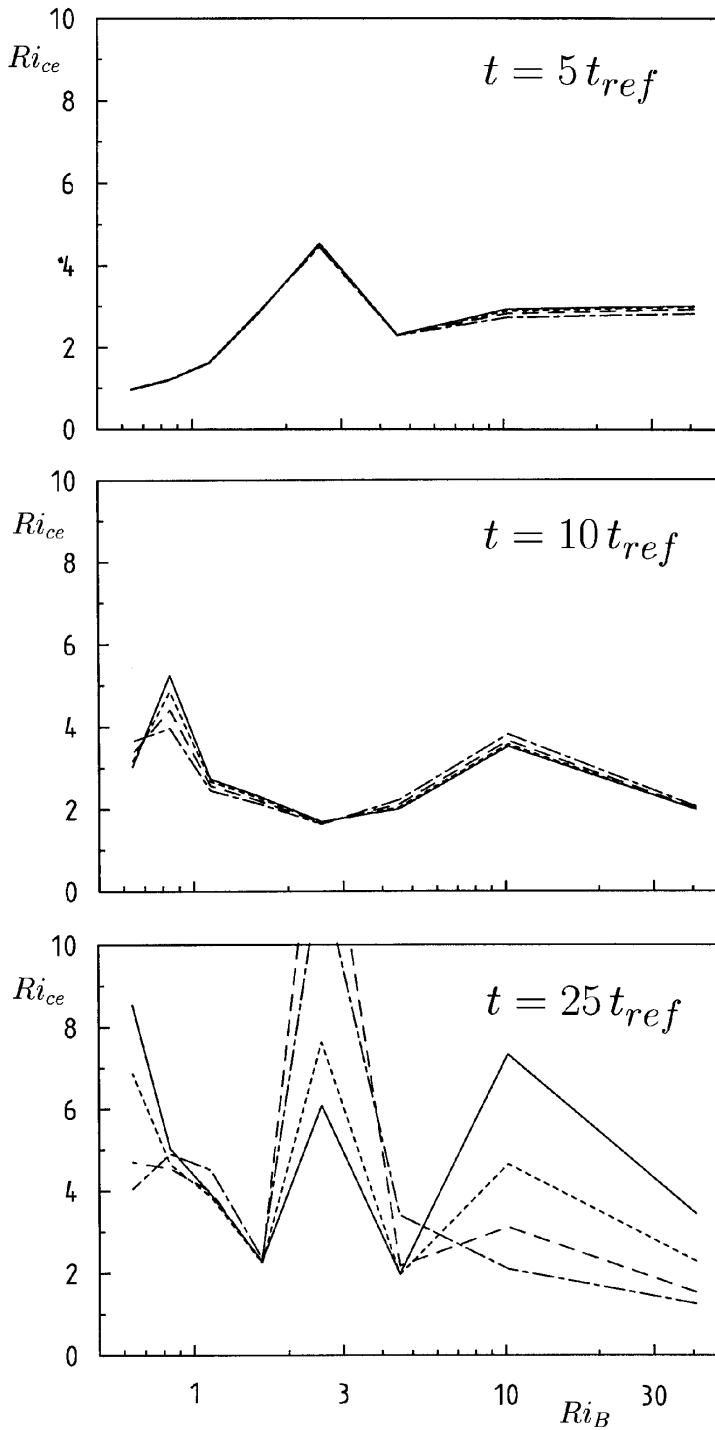


Figure 6. Wave attenuation in terms of the Richardson number Ri_{ce} for different times $t = 5.0 t_{ref}$ (top), $t = 10 t_{ref}$ (middle) and $t = 25 t_{ref}$ (bottom). Line coding as in Figure 5.

from scale or bulk parameters. From Figure 3, an exponential relation between z_{break} and Ri_B is possible. Then assuming complete wave absorption through the critical layer ($z_c - z_{break}$), the stress divergence can be easily estimated. However, this procedure might be limited to simple wavy surfaces.

7. Conclusions

A comparison between a steady linear wave model and a time-dependent nonlinear numerical model has been performed for the case of a linear stratified shear flow over a wavy surface when a critical level is present. Essentially similar results are obtained from each model for wave stress, wave breaking height and wave dissipation through the critical level. Because gravity waves can be either evanescent or internal depending on the relative sizes of the Scorer parameter and the wavenumber of the ground surface disturbance, the somewhat paradoxical result develops that wave breaking and non-linearity increase with increasing bulk Richardson number. It is recommended that steady linear wave theory be used in gravity-wave drag parameterizations provided near real time profiles of background velocity and temperature are available.

Acknowledgements

This work has been supported by the Deutsche Forschungsgemeinschaft and the U.S. Department of Commerce Air Resources Laboratory/NOAA under a grant from the U.S. Department of Energy.

References

- Baines, P. G.: 1995, *Topographic Effects in Stratified Flows*, Cambridge University Press, 482 pp.
- Booker, J. R. and Bretherton, F. P.: 1967, 'The Critical Layer for Internal Gravity Waves in a Shear Flow', *J. Fluid Mech.* **27**, 513–539.
- Delisi, D. P. and Dunkerton, T. J.: 1989, 'Laboratory Observations of Gravity Wave Critical-Layer Flows', *Pure Appl. Geophys.* **130**, 445–461.
- Dörnbrack, A.: 1996, 'Turbulent Mixing by Breaking Gravity Waves', *J. Fluid Mech.* submitted.
- Dörnbrack, A., Gerz, T., and Schumann, U.: 1995, 'Turbulent Breaking of Overturning Gravity Waves Below a Critical Level', *Appl. Scient. Res.* **54**, 163–176.
- Dörnbrack, A. and Schumann, U.: 1993, 'Numerical Simulation of Turbulent Convective Flows Over Wavy Terrain', *Boundary-Layer Meteorol.* **65**, 323–355.
- Eliassen, A. and Palm, E.: 1960, 'On the Transfer of Energy in Stationary Mountain Waves', *Geofysiske Publikasjoner* **XXII**, 1–23.
- Fritts, D. C.: 1984, 'Gravity Wave Saturation in the Middle Atmosphere: A Review of Theory and Observations', *Rev. Geophys. Space Phys.* **22**, 275–308.
- Fritts, D. C. and Geller, M. A.: 1976, 'Viscous Stabilization of Gravity Critical Level Flows', *J. Atmos. Sci.* **33**, 2276–2284.
- Hazel, P.: 1967, 'The Effect of Viscosity and Heat Conduction on Internal Gravity Waves at a Critical Level', *J. Fluid Mech.* **30**, 775–783.

- Kim, Y.-J. and Arakawa, A.: 1995, 'Improvement of Orographic Gravity Wave Parameterization using a Mesoscale Gravity Wave Model', *J. Atmos. Sci.* **52**, 1875–1902.
- Koop, C. G. and McGee, B.: 1986, 'Measurements of Internal Gravity Waves in a Continuously Stratified Shear Flow', *J. Fluid Mech.* **172**, 453–480.
- Nappo, C. J. and André, A.: 1995, 'A Parameterization of Subgrid Scale Gravity-Wave Generated Turbulence in a Mesoscale Boundary Layer Model', *11th Symp. on Boundary Layers and Turbulence*, 27–31 March, Charlotte, NC. American Meteorological Society, Boston, MA, 341–343.
- Nappo, C. J. and Chimonas, G.: 1992, 'Wave Exchange Between the Ground Surface and a Boundary-Layer Critical Level', *J. Atmos. Sci.* **49**, 1075–1091.
- Merrill, J. T. and Grant, J. R.: 1979, 'A Gravity Wave – Critical Level Encounter Observed in the Atmosphere', *J. Geophys. Res.* **84**, 6315–6320.
- Smith, R. B.: 1979, 'The Influence of Mountains on the Atmosphere', *Adv. in Geophysics* **21**, 87–230.
- Thorpe, S. A.: 1968, 'A Method of Producing a Shear Flow in a Stratified Fluid', *J. Fluid Mech.* **32**, 693–704.
- Thorpe, S. A.: 1981, 'An Experimental Study of Critical Layers', *J. Fluid Mech.* **103**, 321–344.
- Worthington, R. M. and Thomas, L.: 1996, 'Radar Measurements of Critical Layer Absorption in Mountain Waves', *Quart. J. Roy. Meteorol. Soc.* **122**, 1263–1282.